

# Strongly correlated exciton-polarons in twisted homo-bilayer heterostructures

Giacomo Mazza<sup>1,2,\*</sup> and Adriano Amaricci<sup>3</sup>

<sup>1</sup>*Dipartimento di Fisica, Università di Pisa, Largo Bruno Pontecorvo 3, 56127, Pisa, Italy*

<sup>2</sup>*Department of Quantum Matter Physics, University of Geneva,  
Quai Ernest-Ansermet 24, 1211 Geneva, Switzerland*

<sup>3</sup>*CNR-IOM, Istituto Officina dei Materiali, Consiglio Nazionale delle Ricerche, Via Bonomea 265, 34136 Trieste, Italy*

We consider dressing of excitonic properties by strongly correlated electrons in gate controlled twisted homo-bilayer heterostructures. The combined effect of the moiré potential and the Coulomb interaction supports the formation of different strongly correlated phases depending on the filling, including charge-ordered metals or incompressible insulators at integer occupation. The coupling between excitons and electrons results in a splitting of the excitonic resonance into an attractive and a repulsive polaron peak. Analyzing the properties of the exciton-polarons across the different phases of the system, we reveal a discontinuous evolution of the spectrum with the formation of a double-peak structure in the repulsive polaron branch. The double-peak structure emerges for non-integer fillings and it is controlled by the energy separation between the quasi-particle states close to the Fermi level and the high-energy doublons excitations. Our results demonstrate that exciton-polarons carry a clear hallmark of the electronic correlations and, thus, provide a direct signature of the formation of correlation driven insulators in gate controlled heterostructures.

The concept of strong correlation is generally used to express the competition between the single- and the many-particles character of the excitation spectrum, which is often at the origin of emerging collective phenomena in quantum many-body systems. In strongly correlated materials this competition, quantified by the relative weight of the electronic kinetic energy and the interaction energy issued from the Coulomb repulsion, can drive a characteristic transition from a metal to a Mott insulator [1]. Yet, more than the metal-insulator transition, a distinctive hallmark of the strongly correlated nature of a material is the existence of concurrent excitations at different energy scales. For instance, long-lived quasi-particles control the low-energy properties of the system whereas incoherent many-body excitations, associated with doublons formation, dominate the higher end of the energy spectrum. This reflects in experimental outcomes, for example by means of direct coupling of the correlated electrons with optical probes [2–5].

In recent years, heterostructures of twisted two-dimensional materials emerged as a new class of electronic systems with tunable correlations thanks to the combined effects of moiré potentials and electrostatic doping [6, 7]. These systems offered a platform to observe a number of phenomena, including metal-insulator transitions, quantum criticality or unconventional superconductivity [6–11]. At the same time, they open new possibilities for detecting signatures of strong correlation, which go beyond the direct spectroscopic response of the correlated electrons [12, 13].

Unlike most correlated materials, heterostructures made of transition-metal dichalcogenide (TMD)s display a semiconducting character in which strongly bounded excitons may act as sensors of correlated electronic states

in the heterostructures [14–19]. The coupling between excitons and the electrons injected by gating can give rise to exciton-polarons (EP), issuing from the dressing of the original exciton resonance by the electronic cloud. In this process new bound states form, known as trions or charged excitons [20–24]. In wideband semiconductors, where Fermi liquid description of conduction electrons applies, the EPs display a blueshift proportional to the density of conduction electrons [22–24]. This description has been used to map the charging diagrams of the TMDs systems and hint at the formation of strongly correlated phases, such as the Wigner crystal in a monolayer MoSe<sub>2</sub> [25] or Mott incompressible states in twisted MoSe<sub>2</sub>/hBN/MoSe<sub>2</sub> heterostructures [14, 15]. Nonetheless, information on the charge density alone may not be conclusive for determining the correlated nature of carriers. Moreover, the standard EP description becomes questionable when Fermi-liquid theory breaks down.

In this paper, we derive a theoretical description of the properties of strongly correlated EPs in a paradigmatic setup of twisted homo-bilayer heterostructures. We obtain a charging diagram characterized by Mott and Wigner-Mott incompressible phases, with a layer-by-layer filling behavior in agreement with the experiments in Ref. [14]. We show that the EP spectrum discontinuously evolves as a function of the electronic density and splits into low- and high-energy branches of excitons dressed, respectively, by the coherent quasi-particles and the incoherent doublons. We predict that for non-integer fillings, the EP spectrum shows multiple resonances at distinct energy scales, highlighting a direct signature of the formation of a correlation-driven Mott insulator.

The rest of this work is organized as follows: in Sec. I we introduce a model describing electrons and excitons dynamics in a twisted homo-bilayer heterostructure. In Sec. II we solve the interacting electrons problem and discuss the formation of different correlated phases at increasing filling. Based on this result, in Sec. III we

\* giacomo.mazza@unipi.it

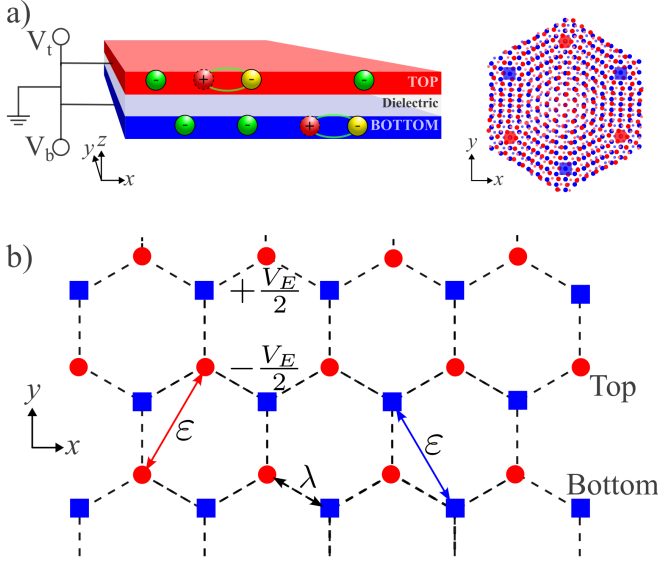


Figure 1. a) Right: Schematic representation of the homo-bilayer heterostructure. Top (red) and Bottom (blue) layers are separated by a dielectric spacer (gray). Bound pairs of negative and positive charges indicate intra-layer excitons. Green charges represent conduction electrons controlled by top  $V_t$  and bottom  $V_b$  gates. Left: Twisted triangular lattices. Dots and squares highlight, respectively, the hexagonal lattice formed by the MX and XM stacking. b) Top view of the lattice structure of the moiré Hamiltonian. Dots/squares sublattices correspond to orbitals localized on top/bottom layers. Arrows indicate the hopping matrix elements. The sublattice potential indicates the perpendicular bias  $V_E$ .

investigate the coupling of electrons with excitons and show how the resulting hybrid exciton-polaron states display hallmarks of strong correlation effects in their spectral properties. Finally, in Sec. IV we draw some conclusions and possible perspectives deriving from our results.

## I. MODEL AND METHODS

We consider two identical monolayers separated by a dielectric spacer (see Fig. 1). The electron doping on each monolayer is controlled via top ( $V_t$ ) and bottom ( $V_b$ ) gates. The monolayers feature well-defined intra-layer exciton resonances. A small twist angle gives rise to a moiré potential, with a periodicity much larger than the monolayer lattice parameter, leading to the formation of flat-bands in the mini-Brillouin zone, which due to the dielectric spacer are characterized by a layer degree of freedom [14, 15, 26, 27]. Moreover, the moiré potential is assumed to be negligible for the intra-layer exciton [28, 29]. Its effect on the excitonic response reduces to the coupling between the intra-layer excitons and the electrons doped into the moiré mini-bands.

We employ a phenomenological description of the electron-exciton problem, valid in the limit of low elec-

tronic density, corresponding to the electronic occupation of the first moiré mini-band with respect to available particle-hole excitations in the wide valence/conduction bands. Our approach builds on the theory of composite many-body excitations in quantum gases mixtures [30–32] which has been successfully applied to the description of trion absorption features in two-dimensional semiconductors [23, 24]. We describe intra-layer excitons as bosonic particles with dispersion  $\omega_{\mathbf{q}}$  and we model their coupling with interacting electrons in terms of the following Hamiltonian:

$$H = H_X + H_{\text{moiré}} + H_{e-X}. \quad (1)$$

where  $H_X = \sum_{\mathbf{q}\alpha=t,b} \omega_{\mathbf{q}} b_{\mathbf{q}\alpha}^\dagger b_{\mathbf{q}\alpha}$  represents the energy of the free exciton gases in the top and bottom layers, respectively  $\alpha = t, b$ .  $H_{\text{moiré}}$  describes the dynamics of the electrons in the moiré lattice and  $H_{e-X}$  is the electron-exciton interaction.

Large scale electronic structure calculations for twisted homo-bilayers TMDs [26] show that the low-energy moiré bands originate from orbital hybridization in a honeycomb lattice formed by the points in which the metal (M) atom of one layer is on top of a chalcogen (X) atom of the other, with opposite layer character for the MX or XM stacking (Fig. 1). Based on that, we model the interacting electrons as an extended Hubbard model on the honeycomb lattice, with the layer index corresponding to the sub-lattice one:

$$H_{\text{moiré}} = -\varepsilon \sum_{ij \in \text{n.n.}} \sum_{\alpha\sigma} c_{i\sigma\alpha}^\dagger c_{j\sigma\alpha} + \lambda \sum_{ij \in \text{n.n.}\sigma} c_{i\sigma t}^\dagger c_{j\sigma b} + h.c. \\ - \mu \sum_{i\sigma\alpha} n_{i\sigma\alpha} + \frac{V_E}{2} \sum_{i\sigma} (n_{i\sigma t} - n_{i\sigma b}) + H_{\text{int}}. \quad (2)$$

where  $\varepsilon$  and  $\lambda$  are, respectively, the intra- and inter-layer hopping between nearest neighbor sites,  $\mu = (V_t + V_b)/2$  is the chemical potential controlling global filling and  $V_E = V_t - V_b$  a perpendicular bias appearing as an effective sublattice potential. In Eq. 2, n.n. and n.n.n. symbols indicate, respectively, nearest and next-nearest neighboring sites. The interaction term contains both the local (intra-layer) density-density interaction  $U$  and the nearest neighbor (inter-layer) one  $U'$ .

$$H_{\text{int}} = U \sum_{i\alpha} n_{i\uparrow\alpha} n_{i\downarrow\alpha} + U' \sum_{ij \in \text{n.n.}} \sum_{\sigma\sigma'} n_{i\sigma t} n_{j\sigma' b}. \quad (3)$$

The local repulsion  $U$  favors Mott localization whereas the non-local term  $U'$  is responsible for Wigner crystallization, which in the present case corresponds to the layer polarization. Here, we focus on a regime in which both mechanisms are at play. We fix  $U = 18\varepsilon$  and  $U' = 0.25U$ , and  $\lambda = 0.2\varepsilon$ , with  $\varepsilon = 0.5\text{meV}$  corresponding to flat-bands of width  $W = 4.5\text{meV}$ . In the rest of this paper, we work at  $T = 0$  and we explicitly discard magnetic ordering.

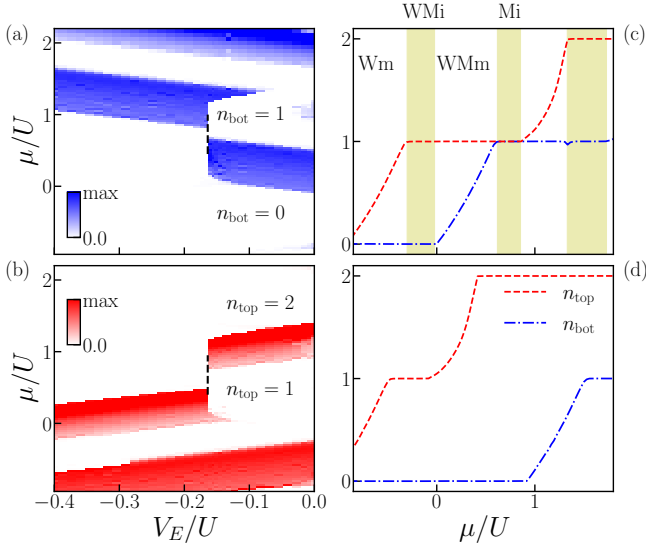


Figure 2. Left Panels. Maps of the charge susceptibility  $\chi_\alpha$ , for the bottom (a) and top (b) layers, as a function of the chemical potential  $\mu$  and interlayer potential  $V_E$ . White areas correspond to charge incompressible regions realized for different fillings. The dashed lines mark the discontinuous transition between incompressible regions at different integer filling. Right Panels. Layer charge densities as a function of  $\mu$  and fixed values of  $V_E/U = -0.08$  (c) and  $V_E/U = -0.25$  (d).

Finally, we assume an effective electron-exciton contact attractive interaction deriving from a charge-dipole polarization mechanism [22–24]

$$H_{e-X} = V_{e-X} \sum_{\mathbf{q}\alpha=t,b} \rho_{\mathbf{q}\alpha}^e \rho_{-\mathbf{q}\alpha}^X \quad (4)$$

where  $\rho_{\mathbf{q}\alpha}^e \equiv \sum_{\mathbf{k}\sigma} c_{\mathbf{k}-\mathbf{q}\sigma\alpha}^\dagger c_{\mathbf{k}\sigma\alpha}$  and  $\rho_{-\mathbf{q}\alpha}^X \equiv \sum_{\mathbf{k}} b_{\mathbf{k}+\mathbf{q}\alpha}^\dagger b_{\mathbf{k}\alpha}$  are, respectively, the electron and the exciton densities on the layer  $\alpha$ . In the following we set  $V_{e-X} = -50$  meV. This value is in line with the estimated short-range electron-exciton interaction in different TMDs [33], and it is found to correctly reproduce the order of magnitude of the experimentally observed polaron shifts [14].

## II. CHARGING DIAGRAM

We first discuss the charging diagram of the heterostructure. We study the electronic Hamiltonian, Eq. 2, by using the Dynamical Mean Field Theory (DMFT) [34] with the Exact Diagonalization algorithm [35] and decoupling of the non-local interaction [36–40]. In Fig. 2, panels (a)-(b), we show maps of the layer charge susceptibilities  $\chi_\alpha \equiv \partial n_\alpha / \partial \mu$ ,  $n_\alpha = \sum_{i\sigma} \langle c_{i\sigma\alpha}^\dagger c_{i\sigma\alpha} \rangle$ , as a function of the chemical potential  $\mu$  and the interlayer bias  $V_E$ . The layer susceptibilities display a characteristic checkerboard pattern, alternating layer-compressible regions ( $\chi_\alpha \neq 0$ ) to layer-

incompressible  $\chi_\alpha = 0$  ones at integer fillings,  $n_\alpha = 0, 1, 2$ . The checkerboard pattern highlights the breaking of the layer symmetry for  $V_E \rightarrow 0$  due to Wigner crystallization. The layer symmetry is restored in a region of the charging diagram characterized by charge densities simultaneously plateauing at half-filling  $n_{\text{top}} = n_{\text{bot}} = 1$ . Panels (c)-(d) show cuts of the layer charge densities  $n_\alpha$  as a function of  $\mu$  for two distinct values of  $V_E$ . The total filling  $n_{\text{tot}} = n_{\text{top}} + n_{\text{bot}}$  increases through a series of compressible and incompressible configurations, indicating the metallic and the insulating character of the heterostructure. The plateaus at  $n_\alpha = 0$  and  $n_\alpha = 2$  correspond, respectively, to completely empty and full bands while those at half-filling  $n_\alpha = 1$  indicate the Mott localized phase.

Depending on the charge configuration  $\nu = (n_{\text{top}}, n_{\text{bot}})$ , we identify different types of correlated phases controlled by the gates. The symmetric configuration,  $\nu = (1, 1)$ , corresponds to the homogeneous Mott insulator (Mi) in which electrons in both layers simultaneously localize.  $\nu = (1, 0)$  represents a Wigner-Mott insulator (WMi) in which saturated charge ordering is concomitant to Mott localization of the charged layer [36–38]. For any non-integer filling  $x$ , the  $\nu = (1, x)$  configuration denotes a Wigner-Mott metal (WMm) in which electrons in the half-filled layer localize whereas electrons in the partially filled layer remain itinerant [37–39]. Finally  $\nu = (x, 0)$  corresponds to a Wigner metal (Wm) with saturated charge ordering and itinerant electrons in the partially filled layer. At larger dopings, charge ordering and Mott localization coexists with completely filled bands, *e.g.*  $\nu = (2, 1)$ . Increasing the bias, the Mi phase disappears in favor of a fully polarized band insulator,  $\nu = (2, 0)$ . Due to the first-order nature of polarization driven Mott transitions [41–43], the bias induced transition is first order, as indicated by dashed lines in panels (a)-(b). Despite the simplicity of the model, the charging diagram highlights a characteristic layer-by-layer filling behavior which reproduces the salient features the charging diagrams reported in [14, 15] for twisted MoSe<sub>2</sub>/hBN/MoSe<sub>2</sub> heterostructures.

## III. EXCITON-POLARONS

We now consider dressing of the excitonic properties caused by coupling to the above strongly correlated electronic phases. For low density the effect of the electrons onto the intra-layer excitons can be treated perturbatively. We are interested in the evolution of the  $\mathbf{q} = 0$  excitonic spectral function as probed by optical spectroscopy [44], *i.e.*  $X_\alpha(\omega) = -\frac{1}{\pi} \text{Im} D_{\mathbf{q}=0\alpha}(\omega)$ , where  $D_{\mathbf{q}\alpha}(\omega) = [\omega + i\eta - \omega_{\mathbf{q}} - \Sigma_{\mathbf{q}\alpha}^X(\omega)]^{-1}$  is the excitonic Green's function expressed in terms of the excitonic self-energy  $\Sigma_{\mathbf{q}\alpha}^X$  function. The latter can be evaluated from the vertex function in the particle-particle channel

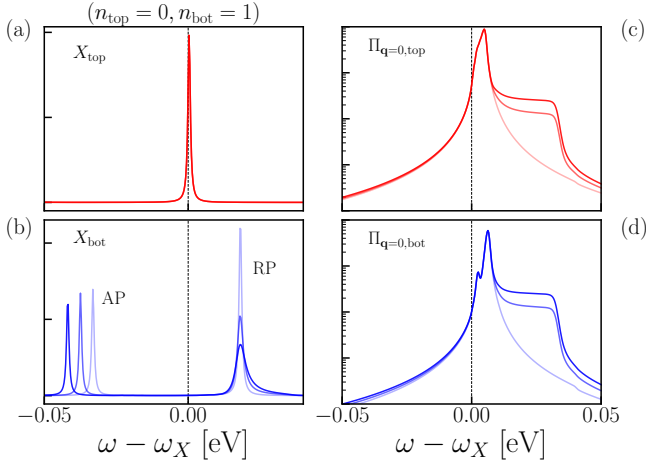


Figure 3. Left panels. Spectral function for top (a) and bottom (b) interlayer excitons corresponding to the charging configuration  $\nu = (0, 1)$ . Frequency is measured with respect to the energy of the bare exciton. Right panels. Imaginary part of the electron-exciton pairing susceptibility at  $\mathbf{q} = 0$  for top (c) and bottom (d) layers. In each panel, the different curves correspond to increasing phenomenological background of electronic spectral density added in the calculations. From light (moiré electrons only) to dark (moiré electrons with phenomenological background) curves. In panel (a) the three curves are indistinguishable.

$\Lambda_{\mathbf{p}\sigma\alpha}$  as [45]

$$\Sigma_{\mathbf{q}\alpha}^X(i\Omega_n) = \sum_{\mathbf{p}\sigma} T \sum_{i\omega_n} G_{\mathbf{p}-\mathbf{q},\sigma\alpha}(i\omega_n) \Lambda_{\mathbf{p}\sigma\alpha}(i\omega_n + i\Omega_n). \quad (5)$$

We compute the vertex  $\Lambda_{\mathbf{p}\sigma\alpha}$  in the ladder approximation [30, 31, 46].

$$\Lambda_{\mathbf{p}\sigma\alpha}(i\omega_n) = V_{e-X} \frac{V_{e-X} \Pi_{\mathbf{p}\sigma\alpha}(i\omega_n)}{1 - V_{e-X} \Pi_{\mathbf{p}\sigma\alpha}(i\omega_n)} \quad (6)$$

and the kernel  $\Pi_{\mathbf{q}\sigma\alpha}$  is the exciton-electron pairing susceptibility

$$\Pi_{\mathbf{q}\sigma\alpha}(i\omega_n) = - \sum_{\mathbf{p}'} T \sum_{i\omega_l} G_{\mathbf{p}-\mathbf{p}',\sigma\alpha}(i\omega_l) D_{\mathbf{p}'\alpha}(i\omega_n - i\omega_l). \quad (7)$$

In these expressions  $i\Omega_n$  and  $i\omega_n$  refer, respectively, to the bosonic and fermionic Matsubara frequencies, while  $G_{\mathbf{k}\sigma\alpha}$  is the interacting electronic Green's function. We assume the electrons act as a bath for the excitons, namely their properties are not affected by photogenerated excitons. The electron propagator  $G_{\mathbf{k}\sigma\alpha}$  is computed in the DMFT approximation using a momentum independent self-energy [34]. Moreover, we compute the pairing susceptibility, Eq. 7, using the bare exciton propagator which we assume having a parabolic dispersion  $\omega_{\mathbf{q}} = \omega_X + \frac{\hbar^2 \mathbf{q}^2}{2M_X}$ . In the following we set a cut-off for the exciton and the electron momenta within the first moiré mini-band.

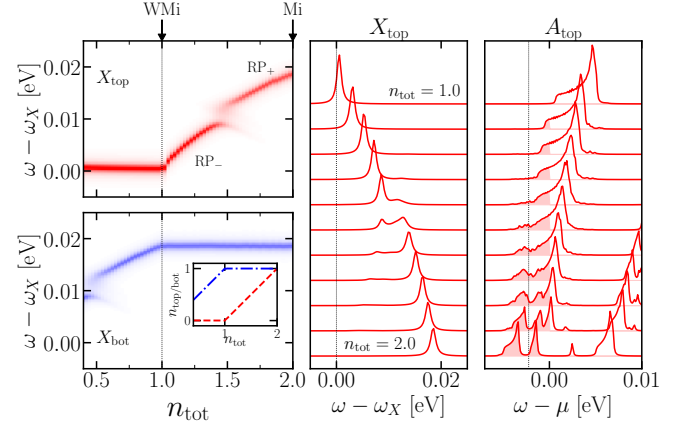


Figure 4. Left panels. Color maps of the top and bottom excitons spectral functions as a function of the total filling  $n_{\text{tot}}$ , the interlayer bias is  $V_E/U = 0.025$ . Inset shows  $n_{\text{top}}$  (dashed line) and  $n_{\text{bot}}$  (dot-dashed line) contributions to the total filling. The arrows and the vertical dotted line indicate the WMi and Mi phases at  $n_{\text{tot}} = 1.0$  and  $n_{\text{tot}} = 2.0$ , respectively. Center panel. Spectral density for the exciton in the top layer at different values of the total filling from  $n_{\text{tot}} = 1.0$  to  $n_{\text{tot}} = 2.0$ . Vertical dotted line represents the bare exciton frequency. Right panel. Electronic spectral density for the top layer for the same fillings in the center panel. Color filling highlights the occupied density of states. Vertical dotted line represents the energy scale  $-(U - W)/2$  (see text) highlighting the formation of the lower Hubbard band.

In Fig. 3, we show the excitonic spectral functions  $X_{\alpha=t,b}$  of the two layers for the  $\nu = (0, 1)$  configuration. For the undoped layer, the spectral function reduces to the bare one with a slightly blue shifted resonance due to the small hybridization  $\lambda$  between the layers. At finite doping, the excitonic resonance splits in two distinct peaks located at energies, respectively, lower and higher than the bare exciton frequency. Such splitting stems from the formation of a pole in the vertex function outside the electron-exciton continuum. The lower energy peak lies below the exciton-electron continuum and represents a bound state, identified as the attractive polaron (AP). The higher energy peak is a scattering state, known as the repulsive polaron (RP).

Polaronic features are known to depend on the energy cut-off of the electron-exciton continuum [22, 24, 32]. Here, we test the dependence of our results with respect to the choice of the cut-off, by adding a small broad background of constant spectral density in the exciton-electron continuum (see Fig. 3 (c) and (d)). In panel (b) of Fig. 3, we show that the position of the AP peak moves with the cut-off whereas the RP is, up to a broadening, essentially cut-off independent. The RP thus represents a genuine feature of the interaction between excitons and the correlated electrons in the first mini-band. In the following, we will restrict our attention to the RP peak as a mean to monitor the effects of strong electronic correlation.



In Fig. 4 we show the evolution of the RP resonance as a function of the total filling through different correlated phases, i.e. from the Wm ( $n_{tot} < 1$ ) to the Mi ( $n_{tot} = 2$ ). In all such cases, the RP resonance undergoes a blue-shift proportional to the density of the electrons, similar to what happens in the more conventional case of exciton-dressing by an electron-gas.

In the correlated electronic phases at non-integer fillings we observe an emerging structure in the RP peak. We follow the top layer exciton in the WMm phase ( $1 < n_{tot} < 2$ ) and observe that the RP resonance splits into two branches originating, respectively, from the empty (RP<sub>-</sub>) and the half-filled layer (RP<sub>+</sub>). Remarkably, the two branches are not continuously connected and appear as two separate peaks for the occupation value  $n_{split} \approx 1.5$ .

From the expression of the exciton self-energy, Eq. 5, we relate the double-peak structure of the RP to the presence of distinct energy scales for the electronic excitations at non-integer fillings. Indeed, frequency convolution in Eq. 5 implies that the excitonic scattering is sensible to the occupied electronic states,  $\text{Im}\Sigma_{top}^X(\omega) \sim -\theta(\omega - \Omega_\Lambda)A_{top}(\Omega_\Lambda - \omega)$  where  $\Omega_\Lambda$  is a characteristic resonance in the vertex function spectral density. Due to the strong correlations, the electronic spectrum,  $A_{top}$  Fig. 4, feature a low-energy quasi-particle resonance close to the Fermi level and higher-energy contributions corresponding to the excitation of doublons.

For small dopings, i.e.  $n_{tot} \simeq 1$ , the electron spectral weight is entirely composed of low-energy quasi-particle excitations, and the spectral density is equivalent to that of the bare triangular lattice. As the filling increases, spectral weight starts to be transferred to the doublons, as highlighted in by the formation of the incoherent Hubbard band for energies  $\omega \lesssim -(U - W)/2 = -2.25$  meV, representing the energy edge of the Hubbard band. This reflects in two separated peaks in  $\text{Im}\Sigma_{top}^X(\omega)$ . The double-peak structure reveals two distinct scattering mechanisms, and manifests into two branches of solutions of the pole equation  $\omega - \omega_X = \text{Re}\Sigma_{top}^X(\omega)$ . We therefore link the RP<sub>-</sub> and RP<sub>+</sub> branches, respectively, with the quasiparticles and the doublons excitations. The avoided crossing occurs when the relative weights of these two electronic excitations become comparable. The splitting is found to increase proportionally to  $U$ . We emphasize that the precise value of the non-integer filling  $n_{split}$  smoothly depends on the model parameters,

e.g. the value of the electron-exciton interaction.

A similar trend can be observed for the bottom layer in the Wm phase  $n_{tot} < 1$ . We conclude that the RP<sub>-</sub> and RP<sub>+</sub> branches bear the hallmark of electronic correlations in the WMm and Wm phases.

#### IV. CONCLUSIONS

We derive a model to describe the coupling of interacting electrons and exciton states in twisted homo-bilayer heterostructures. In particular, by means of DMFT we solved the interacting electrons problem showing that the combination of Coulomb repulsion and gate voltage leads to a characteristic charging diagram, featuring a checker-board pattern of alternating correlated metallic and insulating phases. Using a combination of numerical and analytic methods we treated the electron-exciton coupling to analyze the properties of the EP hybrid states, emerging from strongly correlated electrons dressing the excitons in such systems. We have shown that EP resonances bear the hallmark of strong correlation, namely the coexistence of low-energy quasiparticles and high-energy incoherent excitations. We highlight the discontinuous evolution of the exciton spectrum as filling is varied between a Wigner metal and a Mott insulator. In particular, we predict that, near semi-integer total filling, low- and high-energy features equally participate in the formation of EP states, giving rise to characteristic peaks separated by an energy that depends on the interaction strength. The direct consequence of our findings is that the genuine correlated nature of either metallic or insulating phases in such systems can be immediately identified by means of exciton spectroscopy. Our description can be extended to more specific materials modeling or heterostructure setups for sensing of correlated electrons [47]. Investigating the interplay of inter- and intra-layer interacting excitons [48] is an interesting research direction left for future work.

#### V. ACKNOWLEDGMENTS

We thank M. Fabrizio for useful discussions. This work has been supported by the Swiss National Science Foundation through an AMBIZIONE grant.

- 
- [1] M. Imada, A. Fujimori, and Y. Tokura, Metal-insulator transitions, *Rev. Mod. Phys.* **70**, 1039 (1998).
  - [2] D. N. Basov, R. D. Averitt, D. van der Marel, M. Dressel, and K. Haule, Electrodynamics of correlated electron materials, *Rev. Mod. Phys.* **83**, 471 (2011).
  - [3] A. Comanac, L. de'Medici, M. Capone, and A. J. Millis, Optical conductivity and the correlation strength of high-temperature copper-oxide superconductors, *Nature*

*Physics* **4**, 287 (2008).

- [4] D. Sutter, C. G. Fatuzzo, S. Moser, M. Kim, R. Fittipaldi, A. Vecchione, V. Granata, Y. Sassa, F. Cossalter, G. Gatti, M. Grioni, H. M. Ronnow, N. C. Plumb, C. E. Matt, M. Shi, M. Hoesch, T. K. Kim, T.-R. Chang, H.-T. Jeng, C. Jozwiak, A. Bostwick, E. Rotenberg, A. Georges, T. Neupert, and J. Chang, Hallmarks of hunds coupling in the mott insulator  $\text{Ca}_2\text{RuO}_4$ , *Nature*

**Communications** **8**, 15176 (2017).

- [5] A. Tamai, M. Zingl, E. Rozbicki, E. Cappelli, S. Riccò, A. de la Torre, S. McKeown Walker, F. Y. Bruno, P. D. C. King, W. Meevasana, M. Shi, M. Radović, N. C. Plumb, A. S. Gibbs, A. P. Mackenzie, C. Berthod, H. U. R. Strand, M. Kim, A. Georges, and F. Baumberger, High-resolution photoemission on  $\text{Sr}_2\text{RuO}_4$  reveals correlation-enhanced effective spin-orbit coupling and dominantly local self-energies, *Phys. Rev. X* **9**, 021048 (2019).
- [6] Y. Cao, V. Fatemi, A. Demir, S. Fang, S. L. Tomarken, J. Y. Luo, J. D. Sanchez-Yamagishi, K. Watanabe, T. Taniguchi, E. Kaxiras, R. C. Ashoori, and P. Jarillo-Herrero, Correlated insulator behaviour at half-filling in magic-angle graphene superlattices, *Nature* **556**, 80 (2018).
- [7] Y. Cao, V. Fatemi, S. Fang, K. Watanabe, T. Taniguchi, E. Kaxiras, and P. Jarillo-Herrero, Unconventional superconductivity in magic-angle graphene superlattices, *Nature* **556**, 43 (2018).
- [8] L. Wang, E.-M. Shih, A. Ghiotto, L. Xian, D. A. Rhodes, C. Tan, M. Claassen, D. M. Kennes, Y. Bai, B. Kim, K. Watanabe, T. Taniguchi, X. Zhu, J. Hone, A. Rubio, A. N. Pasupathy, and C. R. Dean, Correlated electronic phases in twisted bilayer transition metal dichalcogenides, *Nature Materials* **19**, 861 (2020).
- [9] A. Ghiotto, E.-M. Shih, G. S. S. G. Pereira, D. A. Rhodes, B. Kim, J. Zang, A. J. Millis, K. Watanabe, T. Taniguchi, J. C. Hone, L. Wang, C. R. Dean, and A. N. Pasupathy, Quantum criticality in twisted transition metal dichalcogenides, *Nature* **597**, 345 (2021).
- [10] Y. Tang, L. Li, T. Li, Y. Xu, S. Liu, K. Barmak, K. Watanabe, T. Taniguchi, A. H. MacDonald, J. Shan, and K. F. Mak, Simulation of hubbard model physics in  $\text{wSe}_2/\text{wS}_2$  moiré superlattices, *Nature* **579**, 353 (2020).
- [11] G. Chen, L. Jiang, S. Wu, B. Lyu, H. Li, B. L. Chittari, K. Watanabe, T. Taniguchi, Z. Shi, J. Jung, Y. Zhang, and F. Wang, Evidence of a gate-tunable mott insulator in a trilayer graphene moiré superlattice, *Nature Physics* **15**, 237 (2019).
- [12] Y. Xie, B. Lian, B. Jäck, X. Liu, C.-L. Chiu, K. Watanabe, T. Taniguchi, B. A. Bernevig, and A. Yazdani, Spectroscopic signatures of many-body correlations in magic-angle twisted bilayer graphene, *Nature* **572**, 101 (2019).
- [13] J. Yang, G. Chen, T. Han, Q. Zhang, Y.-H. Zhang, L. Jiang, B. Lyu, H. Li, K. Watanabe, T. Taniguchi, Z. Shi, T. Senthil, Y. Zhang, F. Wang, and L. Ju, Spectroscopy signatures of electron correlations in a trilayer graphene/hbn moiré superlattice, *Science* **375**, 1295 (2022), <https://www.science.org/doi/pdf/10.1126/science.abg3036>.
- [14] Y. Shimazaki, I. Schwartz, K. Watanabe, T. Taniguchi, M. Kroner, and A. Imamoğlu, Strongly correlated electrons and hybrid excitons in a moiré heterostructure, *Nature* **580**, 472 (2020).
- [15] Y. Shimazaki, C. Kuhlenskamp, I. Schwartz, T. Smoleński, K. Watanabe, T. Taniguchi, M. Kroner, R. Schmidt, M. Knap, and A. M. C. Imamoğlu, Optical signatures of periodic charge distribution in a mott-like correlated insulator state, *Phys. Rev. X* **11**, 021027 (2021).
- [16] G. Wang, A. Chernikov, M. M. Glazov, T. F. Heinz, X. Marie, T. Amand, and B. Urbaszek, Colloquium: Excitons in atomically thin transition metal dichalcogenides, *Rev. Mod. Phys.* **90**, 021001 (2018).
- [17] T. S. Huang, Y.-Z. Chou, C. L. Baldwin, F. Wu, and M. Hafezi, *Mott-moiré excitons* (2022).
- [18] T. C. Berkelbach and D. R. Reichman, Optical and excitonic properties of atomically thin transition-metal dichalcogenides, *Annual Review of Condensed Matter Physics* **9**, 379 (2018), <https://doi.org/10.1146/annurev-conmatphys-033117-054009>.
- [19] Y. Xu, S. Liu, D. A. Rhodes, K. Watanabe, T. Taniguchi, J. Hone, V. Elser, K. F. Mak, and J. Shan, Correlated insulating states at fractional fillings of moiré superlattices, *Nature* **587**, 214 (2020).
- [20] J. S. Ross, S. Wu, H. Yu, N. J. Ghimire, A. M. Jones, G. Aivazian, J. Yan, D. G. Mandrus, D. Xiao, W. Yao, and X. Xu, Electrical control of neutral and charged excitons in a monolayer semiconductor, *Nature Communications* **4**, 1474 (2013).
- [21] K. F. Mak, K. He, C. Lee, G. H. Lee, J. Hone, T. F. Heinz, and J. Shan, Tightly bound trions in monolayer  $\text{MoS}_2$ , *Nature Materials* **12**, 207 (2013).
- [22] D. K. Efimkin and A. H. MacDonald, Many-body theory of trion absorption features in two-dimensional semiconductors, *Phys. Rev. B* **95**, 035417 (2017).
- [23] D. K. Efimkin, E. K. Laird, J. Levinsen, M. M. Parish, and A. H. MacDonald, Electron-exciton interactions in the exciton-polaron problem, *Phys. Rev. B* **103**, 075417 (2021).
- [24] M. Sidler, P. Back, O. Cotlet, A. Srivastava, T. Fink, M. Kroner, E. Demler, and A. Imamoğlu, Fermi polaron-polaritons in charge-tunable atomically thin semiconductors, *Nature Physics* **13**, 255 (2017).
- [25] T. Smoleński, P. E. Dolgirev, C. Kuhlenskamp, A. Popert, Y. Shimazaki, P. Back, X. Lu, M. Kroner, K. Watanabe, T. Taniguchi, I. Esterlis, E. Demler, and A. Imamoğlu, Signatures of wigner crystal of electrons in a monolayer semiconductor, *Nature* **595**, 53 (2021).
- [26] Y. Zhang, T. Liu, and L. Fu, Electronic structures, charge transfer, and charge order in twisted transition metal dichalcogenide bilayers, *Phys. Rev. B* **103**, 155142 (2021).
- [27] C. Kuhlenskamp, W. Kadow, A. Imamoğlu, and M. Knap, *Tunable topological order of pseudo spins in semiconductor heterostructures* (2022).
- [28] S. Shabani, D. Halbertal, W. Wu, M. Chen, S. Liu, J. Hone, W. Yao, D. N. Basov, X. Zhu, and A. N. Pasupathy, Deep moiré potentials in twisted transition metal dichalcogenide bilayers, *Nature Physics* **17**, 720 (2021).
- [29] C. Linderälv, J. Hagel, S. Brem, E. Malic, and P. Erhart, *The moiré potential in twisted transition metal dichalcogenide bilayers* (2022).
- [30] P. Massignan, M. Zaccanti, and G. M. Bruun, Polarons, dressed molecules and itinerant ferromagnetism in ultracold fermi gases, *Reports on Progress in Physics* **77**, 034401 (2014).
- [31] R. Combescot, A. Recati, C. Lobo, and F. Chevy, Normal state of highly polarized fermi gases: Simple many-body approaches, *Phys. Rev. Lett.* **98**, 180402 (2007).
- [32] F. Chevy, Universal phase diagram of a strongly interacting fermi gas with unbalanced spin populations, *Phys. Rev. A* **74**, 063628 (2006).
- [33] C. Fey, P. Schmelcher, A. Imamoğlu, and R. Schmidt, Theory of exciton-electron scattering in atomically thin semiconductors, *Phys. Rev. B* **101**, 195417 (2020).
- [34] A. Georges, G. Kotliar, W. Krauth, and M. J. Rozenberg, Dynamical mean-field theory of strongly correlated

- fermion systems and the limit of infinite dimensions, *Rev. Mod. Phys.* **68**, 13 (1996).
- [35] A. Amaricci, L. Crippa, A. Scazzola, F. Petocchi, G. Mazza, L. de Medici, and M. Capone, Edipack: A parallel exact diagonalization package for quantum impurity problems, *Computer Physics Communications* **273**, 108261 (2022).
  - [36] A. Camjayi, K. Haule, V. Dobrosavljević, and G. Kotliar, Coulomb correlations and the wigner-mott transition, *Nature Physics* **4**, 932 (2008).
  - [37] A. Amaricci, A. Camjayi, K. Haule, G. Kotliar, D. Tanasković, and V. Dobrosavljević, Extended hubbard model: Charge ordering and wigner-mott transition, *Phys. Rev. B* **82**, 155102 (2010).
  - [38] J. Merino, A. Ralko, and S. Fratini, Emergent heavy fermion behavior at the wigner-mott transition, *Phys. Rev. Lett.* **111**, 126403 (2013).
  - [39] K. J. Kapcia, S. Robaszkiewicz, M. Capone, and A. Amaricci, Doping-driven metal-insulator transitions and charge orderings in the extended hubbard model, *Phys. Rev. B* **95**, 125112 (2017).
  - [40] Y. Tan, P. K. H. Tsang, V. Dobrosavljević, and L. Rademaker, *Doping a wigner-mott insulator: Electron slush in transition-metal dichalcogenide moiré heterobilayers* (2022).
  - [41] P. Werner and A. J. Millis, High-spin to low-spin and orbital polarization transitions in multiorbital mott systems, *Phys. Rev. Lett.* **99**, 126405 (2007).
  - [42] A. Amaricci, J. C. Budich, M. Capone, B. Trauzettel, and G. Sangiovanni, First-order character and observable signatures of topological quantum phase transitions, *Phys. Rev. Lett.* **114**, 185701 (2015).
  - [43] G. Mazza, A. Amaricci, M. Capone, and M. Fabrizio, Field-driven mott gap collapse and resistive switch in correlated insulators, *Phys. Rev. Lett.* **117**, 176401 (2016).
  - [44] I. Amelio, L. Korosec, I. Carusotto, and G. Mazza, Optical dressing of the electronic response of two-dimensional semiconductors in quantum and classical descriptions of cavity electrodynamics, *Phys. Rev. B* **104**, 235120 (2021).
  - [45] In the self-energy we neglect the Hartree shift contribution that would produce a featureless red-shift of the exciton level. Indeed, we assume this contribution is counterbalanced by other effects, e.g. increase of the exciton energy due to screening, which are beyond the scope of the phenomenological model.
  - [46] M. Randeria, J.-M. Duan, and L.-Y. Shieh, Bound states, cooper pairing, and bose condensation in two dimensions, *Phys. Rev. Lett.* **62**, 981 (1989).
  - [47] W. Li, L. M. Devenica, J. Zhang, Y. Zhang, X. Lu, K. Watanabe, T. Taniguchi, A. Rubio, and A. Srivastava, *Local sensing of correlated electrons in dual-moiré heterostructures using dipolar excitons* (2021).
  - [48] I. Amelio, N. Drummond, E. Demler, R. Schmidt, and A. Imamoglu, *Polaron spectroscopy of a bilayer excitonic insulator* (2022).